Improving the intensity and efficiency of compressed echo in rare-earth-ion-doped crystal*

Xiu-Rong Ma(马秀荣)[1,2], Yu-Qing Liang(梁裕卿)[1,†], Song Wang(王松)[1], Shuang-Gen Zhang(张双根)[1,2], and Yun-Long Shan(单云龙)[1]

[1] *Department of Computer and Communication Engineering, Tianjin University of Technology, Tianjin* 300384, *China*
[2] *Engineering Research Center of Communication Devices and Technology, Ministry of Education; Tianjin Key Laboratory of Film Electronic and Communication Devices, Tianjin* 300384, *China*

(Received 11 October 2015; revised manuscript received 22 January 2016; published online 9 June 2016)

We investigate the intensity and efficiency of a compressed echo, which is important in arbitrary waveform generation (AWG). A new model of compressed echo is proposed based on the optical Bloch equations, which exposes much more detailed parameters than the conventional model, such as the time delay of the chirp lasers, the nature of the rare-earth-ion-doped crystal, etc. According to the novel model of compressed echo, we find that reducing the time delay of the chirp lasers and scanning the lasers around the center frequency of the inhomogeneously broadened spectrum, while utilizing a crystal with larger coherence time and excitation lifetime can improve the compressed echo's intensity and efficiency. The theoretical analysis is validated by numerical simulations.

Keywords: intensity and efficiency, compressed echo, arbitrary waveform generation, optical Bloch equations

PACS: 03.65.Sq, 14.70.Bh, 34.80.Pa, 42.50.Md **DOI:** 10.1088/1674-1056/25/7/070302

1. Introduction

The three-pulse photon echo (3PE) is a well-known technique which is applied to arbitrary waveform generation (AWG) and stores intense light pulses by a rare-earth-ion-doped crystal (REIC).[1–4] Compared to the traditional waveform generation methods, this AWG technology enjoys unrivaled capabilities in terms of processing bandwidth and time-to-bandwidth product (TBP). According to the 3PE mechanism, the compressed echo sequences are generated by REIC and can be controlled to change their shapes by adjusting the chirp lasers, thus forming AWG. This technique can generate $\sim$GHz/s bit rate codes with fantastic $\sim 10^5$ TBP, such as an ASC-II code,[5] a periodic Barker code,[6,7] and a pulse-position-modulation code.[8] Several successful cases of AWG based on the 3PE technology have been demonstrated. Meanwhile research for the improvements of 3PE's intensity and efficiency is continuing.

In most previous papers, the stimulated 3PE response is extensively written as the convolution product of the three input pulses' driving fields (Eq. (2) of Ref. [3]). The intensity and phase of each input pulse can be controlled to change the echoes' shape. This expression is simple but it ignores the relationship between the delay time of the pulses and the relaxation time which may influence the 3PE's performance. In Ref. [9], Sangouard *et al.* proposed a model of photon echo based on Ref. [10]. They calculated the macroscopic polarization of the 3PE to obtain its intensity and efficiency. However, this model does not provide clear information about the signal field's change and the relaxation time limitation which is caused by the coherent transient effect (Eq. (8) of Ref. [9]) as well. In order to make the precise control of the input pulses for improving the intensity and efficiency of 3PE, it is essential to rewrite the expression of the 3PE response in other ways.

In this paper, we consider the REIC as a thin medium and present a theoretical model for compressed echo generation in a two-level system by using the optical Bloch equations. The compressed echo can be regarded as the aggregation of numerous single photon echoes which occur from f_{s1} to $f_{s1}+B$.[2,4] Therefore, we first deduce the expression of a single photon echo and verify that the larger time delay of the input pulses will decrease the echo's intensity. Furthermore, the efficiency of the photon echo is a sine-like function with the increase of the rephasing pulse's area and optical thickness. Then, we establish the relationship between the single photon echo and the compressed echo. Compared with the conventional model of compressed echo, the novel model exposes much more detailed parameters which can be controlled in practice. According to the novel model of compressed echo, reducing the time delay of the chirp lasers and the scanning lasers around the center frequency of the inhomogeneously broadened spectrum while utilizing the crystal with larger coherence time and excitation lifetime can improve the intensity and efficiency of the compressed echo, which makes the 3PE technology more suitable for AWG.[5–8] Finally, the theoretical analysis is validated by numerical simulations.

*Project supported by Special Funds for Scientific and Technological Innovation Projects in Tianjin, China (Grant No. 10FDZDGX00400) and the Tianjin Research Program of Application Foundation and Advanced Technology, China (Grant No. 15JCQNJC01100).

†Corresponding author. E-mail: airforce094@sina.com

© 2016 Chinese Physical Society and IOP Publishing Ltd

2. Basic model

This section consists of two parts. We will start from the model of 3PE based on Bloch equations and analyze the factors which have influence on the echo's intensity and efficiency. Then we will establish the relationship between 3PE and the compressed echo, and propose several methods to improve the compressed echo's intensity and efficiency.

2.1. The model of 3PE based on optical Bloch equations

The coherent effect of pulses on a system of inhomogeneously broadened two-level atoms is given by Bloch's equations, where the electric field acts as a source for the atomic dipoles.[11] The Bloch equations govern the coherent lossless interaction of light pulses and atomic dipoles, and are given as[12]

$$\dot{u} = -\Delta v - u(t)/T_2, \tag{1a}$$

$$\dot{v} = \Delta u + R_0 w - v(t)/T_2, \tag{1b}$$

$$\dot{w} = -R_0 v - \left[w(t) - w^0\right]/T_1, \tag{1c}$$

where u, v, and w are the dispersion, absorption, and population inversion components of the Bloch vectors; $\Delta = \omega_{ab} - \omega_0$ is the frequency detuning, which is the difference between the atom's resonant frequency ω_{ab} and the laser frequency ω_0; $|R_0|$ is the Rabi frequency, which is defined by $R_0 = \wp E_0/\hbar$, $\wp = 10^{-29}$ C·m is the dipole matrix element of the transition, and $\hbar$ is the Planck constant; T_1 is the population lifetime; T_2 is the coherence time of the crystal; and w^0 is the balance value of population inversion.

The 3PE will appear at t_{3PE} when three laser pulses with ultrashort time width are shot into the crystal successively, as shown in Fig. 1. Each laser pulse has a coherent interaction with the crystal including optical nutation process and free induction decay process.

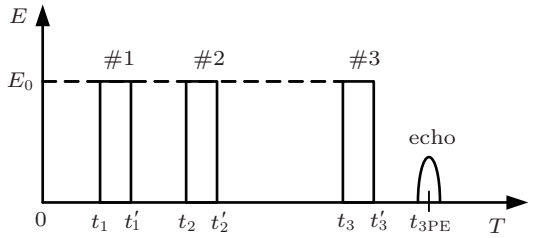


Fig. 1. Basic mechanism of 3PE. The first pulse #1 interacts with the medium from t_1 to t_1'. The next two pulses #2 and #3 are applied from t_2 to t_2' and from t_3 to t_3', respectively. The echo is expected at time $t_{3PE} = t_3' + (t_2 - t_1')$.

At time t_1, the Bloch vectors are set as $u(t_1)$=$v(t_1)$=0 and $w(t_1)$=−1. Consider that the time width of the input pulses is far less than T_1, T_2, and the input pulses are strictly resonant, namely, $\Delta \approx 0$, thus the Bloch vectors during $t_1 < t \le t_1'$ can be expressed as

$$u(t) = u(t_1) = 0, \tag{2a}$$

$$v(t) = R_0 w(t_1) \sin(Rt)/R, \tag{2b}$$

$$w(t) = w(t_1) + R_0^2 w(t_1) \left[\cos(Rt) - 1\right]/R^2, \tag{2c}$$

where $R = \left(R_0^2 + \Delta^2\right)^{1/2}$ is the generalized Rabi frequency and Rt is defined as the area of input pulse.

The signal field in pulse #1's optical nutation is given by

$$E_{n1}(z,t) = AR_0 w(t_1) \frac{e^{-(\Delta/\Delta\omega)^2}}{\sqrt{\pi}\Delta\omega} J_0(R_0 t)\, e^{-t/T_2} e^{i(\omega t - kz)}, \tag{3}$$

where $A = \wp N_{atom} LK/2\varepsilon$, here $N_{atom} = 10^{24}$ m^{-3} is the total number of atoms, L is the thickness of the crystal,[13] $K = \omega_0/c$ is the wave number, and $\varepsilon = 8.85 \times 10^{-12}$ F/m is the dielectric constant, $J_0(R_0 t)$ is the zeroth-order Bessel function with Rabi frequency R_0, $\delta\omega_D$ is the inhomogeneous width, and k is the wave vector.

The Bloch vectors of pulse #1 during free induction decay $t_1' < t \le t_2$ are written as

$$\begin{aligned} u(t) &= \left\{u(t_1')\cos\left[\Delta'(t-t_1')\right] \right. \\ &\quad \left. - v(t_1')\sin\left[\Delta'(t-t_1')\right]\right\} e^{-(t-t_1')/T_2} \\ &= -\left[R_0 w(t_1)/R\right]\sin\left(Rt_1'\right)\sin\left[\Delta'(t-t_1')\right] e^{-(t-t_1')/T_2}, \end{aligned} \tag{4a}$$

$$\begin{aligned} v(t) &= \left\{u(t_1')\sin\left[\Delta'(t-t_1')\right] \right. \\ &\quad \left. + v(t_1')\cos\left[\Delta'(t-t_1')\right]\right\} e^{-(t-t_1')/T_2} \\ &= \left[R_0 w(t_1)/R\right]\sin\left(Rt_1'\right)\cos\left[\Delta'(t-t_1')\right] e^{-(t-t_1')/T_2}, \end{aligned} \tag{4b}$$

$$\begin{aligned} w(t) &= w^0 + \left[w(t_1') - w^0\right] e^{-(t-t_1')/T_1} \\ &= w^0 + \left[w(t_1)\cos\left(Rt_1'\right) - w^0\right] e^{-(t-t_1')/T_1}, \end{aligned} \tag{4c}$$

where $\Delta' = \Delta + \delta\omega$, and $\delta\omega$ is the frequency shift of the atoms.

In the calculation, we note[14]

$$\begin{aligned} &\int_{-\infty}^{\infty} \cos\left[\Delta'\left(t-t_1'\right)\right] e^{-(\Delta/\delta\omega_D)^2} d\Delta \\ &\approx \cos\left[\delta\omega\left(t-t_1'\right)\right]\sqrt{\pi}\delta\omega_D e^{\frac{-(t-t_1')^2\delta\omega_D^2}{4}}. \end{aligned} \tag{5}$$

Therefore, the signal field in pulse # 1's free induction decay can be written as

$$\begin{aligned} E_{d1}(t) &\approx A\left[R_0 w(t_1)/R\right]\cos\left[\delta\omega\left(t-t_1'\right)\right] e^{-(t-t_1')/T_2} \\ &\quad \times \sin\left(Rt_1'\right) e^{\frac{-(t-t_1')^2\delta\omega_D^2}{4}}. \end{aligned} \tag{6}$$

Similarly, the input pulse #2 has optical nutation and free induction decay processes as well. The Bloch vectors during $t_2 < t \le t_2'$ can be expressed as

$$u(t) = u(t_2), \tag{7a}$$

$$\begin{aligned} v(t) &= v(t_2)\cos\left[R(t_2'-t_2)\right] \\ &\quad + \sin\left[R(t_2'-t_2)\right]\left[\Delta u(t_2) + R_0 w(t_2)\right]/R, \end{aligned} \tag{7b}$$

$$\begin{aligned} w(t) &= w(t_2) - R_0 v(t_2)\sin\left[R(t_2'-t_2)\right]/R \\ &\quad + R_0\left[\Delta u(t_2) + R_0 w(t_2)\right]\left\{\cos\left[R(t_2'-t_2)\right] - 1\right\}/R^2. \end{aligned} \tag{7c}$$

The signal field in pulse #2's optical nutation during $t_2 < t \le t_2'$ can be written as

$$\begin{aligned} E_{\rm n2}(z,t) &= A\,{\rm e}^{-(t_2-t_1')/T_2}\,{\rm e}^{{\rm i}(\omega t-kz)}\{R_0 w(t_1)/R \\ &\times \cos\left[\delta\omega\left(t_2-t_1'\right)\right]\sin\left(Rt_1'\right){\rm e}^{-\frac{(t_2-t_1')^2\delta\omega_{\rm D}^2}{4}} \\ &\times \cos\left[R\left(t-t_2\right)\right]+R_0 w(t_2)J_0\left[R_0\left(t-t_2\right)\right]\}. \end{aligned} \tag{8}$$

Afterwards, pulse #2 undergoes the free induction decay and its Bloch vectors are given by

$$\begin{aligned} u(t) &= \{u(t_2')\cos[\Delta'(t-t_2')] \\ &\quad -v(t_2')\sin[\Delta'(t-t_2')]\}\,{\rm e}^{-(t-t_2')/T_2}, \qquad (9a) \\ v(t) &= \{u(t_2')\sin[\Delta'(t-t_2')] \\ &\quad +v(t_2')\cos\left[\Delta'(t-t_2')\right]\}\,{\rm e}^{-(t-t_2')/T_2}, \qquad (9b) \\ w(t) &= w^0+[w(t_2')-w^0]\,{\rm e}^{-(t-t_2')/T_1}. \qquad (9c) \end{aligned}$$

Imitating the calculation method of pulse # 1, the signal field in pulse # 2's free induction decay can be written as

$$\begin{aligned} E_{\rm d2}(t) &= A\,{\rm e}^{-(t-t_2')/T_2}\sin\left(Rt_1'\right){\rm e}^{-(t_2-t_1')/T_2}R_0 w(t_1)/R \\ &\times\left\{\frac{1}{2}\cos\left[\delta\omega\left(t_2-t_1'+t-t_2'\right)\right]{\rm e}^{-\frac{(t_2-t_1'+t-t_2')^2\delta\omega_{\rm D}^2}{4}}\right. \\ &-\frac{1}{2}\cos\left[\delta\omega\left(t_2-t_1'-t+t_2'\right)\right]{\rm e}^{-\frac{(t_2-t_1'-t+t_2')^2\delta\omega_{\rm D}^2}{4}} \\ &+\frac{1}{2}\cos\left[\delta\omega\left(t_2-t_1'+t-t_2'\right)\right]{\rm e}^{-\frac{\left(t_2-t_1'+t-t_2'\right)^2\delta\omega_{\rm D}^2}{4}} \\ &\times\cos\left[R(t_2'-t_2)\right] \\ &+\frac{1}{2}\cos\left[\delta\omega\left(t_2-t_1'-t+t_2'\right)\right]{\rm e}^{-\frac{\left(t_2-t_1'-t+t_2'\right)^2\delta\omega_{\rm D}^2}{4}} \\ &\left.\times\cos\left[R(t_2'-t_2)\right]\right\}. \end{aligned} \tag{10}$$

The third input pulse #3 has the same processes as the former two. During the optical nutation process, namely, $t_3 < t \le t_3'$, the Bloch vectors are given by

$$\begin{aligned} u(t) &= u(t_3), \qquad (11a) \\ v(t) &= v(t_3)\cos[R(t-t_3)] \\ &\quad +[\Delta u(t_3)+R_0 w(t_3)]\sin[R(t-t_3)]/R \\ &= v(t_3)\cos[R(t-t_3)]+R_0 w(t_3)\sin[R(t-t_3)]/R, \qquad (11b) \\ w(t) &= w(t_3)-R_0 v(t_3)\sin[R(t-t_3)]/R \\ &\quad +R_0[\Delta u(t_3)+R_0 w(t_3)]\{\cos[R(t-t_3)]-1\}/R^2. \qquad (11c) \end{aligned}$$

The signal field in pulse #3's optical nutation can be expressed as

$$\begin{aligned} &E_{\rm n3}(z,t) \\ &= A\left\{R_0 w(t_3)J_0\left(R_0\left(t-t_3\right)\right)\right. \\ &+[R_0 w(t_1)/R]\cos[R(t-t_3)]\,{\rm e}^{-(t_3-t_2'+t_2-t_1')/T_2}\sin\left(Rt_1'\right) \\ &\times\left\{\left[\frac{1}{2}+\frac{\cos\left(R(t_2'-t_2)\right)}{2}\right]\cos\left[\delta\omega\left(t_3-t_2'+t_2-t_1'\right)\right]\right. \\ &\times{\rm e}^{-\frac{(t_3-t_2'+t_2-t_1')^2\delta\omega_{\rm D}^2}{4}}+\left[\frac{1}{2}+\frac{\cos\left(R(t_2'-t_2)\right)}{2}\right] \\ &\times\cos\left[\delta\omega\left(t_3-t_2'-t_2+t_1'\right)\right]{\rm e}^{-\frac{(t_3-t_2'-t_2+t_1')^2\delta\omega_{\rm D}^2}{4}}\Big\}\Big\} \\ &\times{\rm e}^{{\rm i}(\omega t-kz)}. \end{aligned} \tag{12}$$

The Bloch vectors in the free induction decay process can be written as

$$\begin{aligned} u(t) &= \{u(t_3')\cos[\Delta'(t-t_3')] \\ &\quad -v(t_3')\sin[\Delta'(t-t_3')]\}\,{\rm e}^{-(t-t_3')/T_2}, \qquad (13a) \\ v(t) &= \{u(t_3')\sin[\Delta'(t-t_3')] \\ &\quad +v(t_3')\cos[\Delta'(t-t_3')]\}\,{\rm e}^{-(t-t_3')/T_2}, \qquad (13b) \\ w(t) &= w^0+[w(t_3')-w^0]\,{\rm e}^{-(t-t_3')/T_1}. \qquad (13c) \end{aligned}$$

The photon echo will appear at time $t_{3\rm PE} = t_3'+(t_2-t_1')$ during the last free induction decay process. Substitute all the above Bloch vectors into Eq. (13b) and take $\sin\left(\Delta'\left(t-t_{3\rm PE}\right)\right)=0$ into account in the deduction. The signal field of 3PE can be written as

$$\begin{aligned} E_{3\rm PE}(t) &= -A\left[R_0^3/R^3\right]w\left(t_1\right)\sin\left(Rt_1'\right)\sin\left[R\left(t_2'-t_2\right)\right] \\ &\times\sin\left[R\left(t_3'-t_3\right)\right]\cos\left[\delta\omega\left(t-t_{3\rm PE}\right)\right]{\rm e}^{-(t_3-t_2')/T_1} \\ &\times\left({\rm e}^{-\left(t-t_3'\right)/T_2}\,{\rm e}^{-\left(t_2-t_1'\right)/T_2}\right){\rm e}^{-\frac{(t-t_{3\rm PE})^2\delta\omega_{\rm D}^2}{4}}. \end{aligned} \tag{14}$$

When the areas of these three pulses satisfy

$$Rt_1' = R\left(t_2'-t_2\right) = R\left(t_3'-t_3\right) = \pi/2, \tag{15}$$

and $t_{3\rm PE} = t_3'+(t_2-t_1')$, the signal field of 3PE obtains its maximum

$$\begin{aligned} &E_{3\rm PE}(t_{3\rm PE}) \\ &= -A\left[R_0^3/R^3\right]w\left(t_1\right)\left({\rm e}^{-(t_3-t_2')/T_1}\,{\rm e}^{-2\left(t-t_3'\right)/T_2}\right). \end{aligned} \tag{16}$$

Assume that the time width of each input pulse is 5 ns, which is much shorter than the population lifetime T_1 and the coherence time T_2. As shown in Fig. 2, these three input pulses shot into the crystal at 0 ns, 15 ns, and 50 ns, respectively. Then the 3PE will appear at $t_{3\rm PE} = t_3'+(t_2-t_1') = 55+(15-5) = 65$ ns.

According to Eq. (16), we can obtain several important factors about the intensity and efficiency of 3PE. The time delay between pulse #1 and pulse #2, and the time delay between pulse #2 and pulse #3 determine the photon echo's intensity. The relationship between the photon echo's intensity and the time delay can be written as

$$I_{\rm echo}^{\rm MAX} = \left|E_{3\rm PE}\left(t_{3\rm PE}\right)\right|^2 \propto \left({\rm e}^{-2\left(t_2-t_1'\right)/T_2}\,{\rm e}^{-(t_3-t_2')/T_1}\right)^2. \tag{17}$$

The time delay (t_2-t_1') is limited by T_2 and the time delay (t_3-t_2') is limited by T_1.

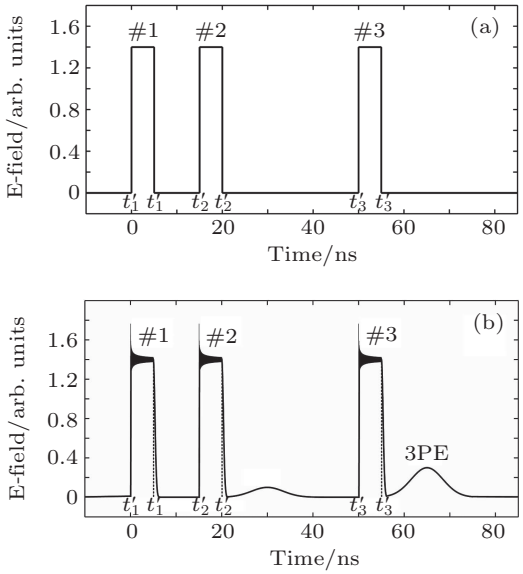


Fig. 2. Short rectangle-pulse photon echo simulation. (a) Three rectangle pulses with 5 ns timewidth shot into REIC at 0 ns, 15 ns, and 50 ns respectively. (b) The whole process of 3PE's optical coherent transient effect.

As shown in Fig. 3, the intensity of 3PE follows a product of two exponential decays, which is in good agreement with Eq. (4.1) of Ref. [15].

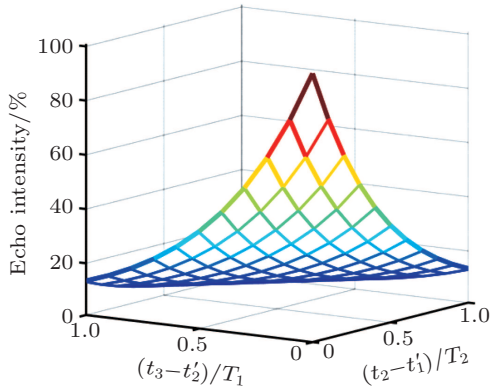


Fig. 3. (color online) Relationship between the intensity of 3PE and the delay time of the input pulses. The coherence time T_2 of the crystal is usually 1–100 ms and the population lifetime T_1 of the crystal is usually ~ 10 ms.

The read out efficiency of the photon echo is easily obtained as

$$\eta_{\text{echo}} = I_{\text{echo}}^{\text{MAX}}/I_{\text{n1}} = |E_{\text{3PE}}(t)|_{t=t_{\text{3PE}}}|^2/|E_{\text{n1}}(z,t)|_{z=L,t=t_1'}|^2. \quad (18)$$

According to Beer's law,

$$I_{\text{n1}} = E_{\text{n1}}^2(z,t) = E_{\text{n1}}^2(0,t)\,\text{e}^{-\alpha z}. \quad (19)$$

Substituting Eqs. (3), (16), and (19) into Eq. (18), we have

$$\eta_{\text{echo}} = I_{\text{echo}}^{\text{MAX}}/I_{\text{n1}} = |E_{\text{3PE}}(t)|_{t=t_{\text{3PE}}}|^2/|E_{\text{n1}}(0,t)|_{t=t_1'}|^2\,\text{e}^{-\alpha L}, \quad (20)$$

where α is the absorption coefficient of the medium.

In Eq. (20), input pulse #1 and pulse #2 are set as $\pi/2$ pulses. The area of rephasing pulse #3 changes from 0 to π. For different optical thickness αL, we plot the efficiency as a function of the rephasing pulse #3's area in Fig. 4. We observe that the efficiency is strongly dependent on the optical thickness. When the optical thickness is small, the efficiency is essentially weak since the signal is poorly absorbed. The efficiency is then a sine-like function with the increase of pulse #3's area. On the other hand, with a larger optical thickness, the efficiency can be much larger than unity and obtains its maximum when the pulse #3's area is $\pi/2$.

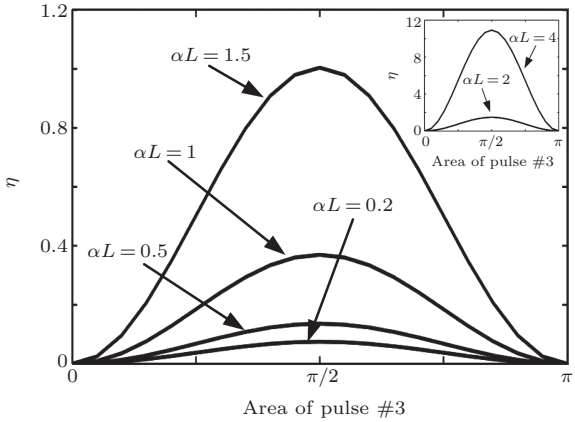


Fig. 4. Efficiency of 3PE as a function of rephasing pulse #3's area for different optical thickness αL. Inset: for larger αL, the maximum efficiency is much larger than unity.

2.2. The model of compressed echo on arbitrary waveform generation

The arbitrary waveform generation based on 3PE is popularly used in optical communication and different signals' generation. The arbitrary waveform consists of compressed echo sequences whose intensity and phase can be controlled by the chirp lasers. To achieve a compressed photon echo, three different linear chirp lasers are shot into an REIC. A spectral grating can be formed in the inhomogeneous broadened absorption profile when two temporally overlapping linear frequency chirps are overlapped within the REIC.

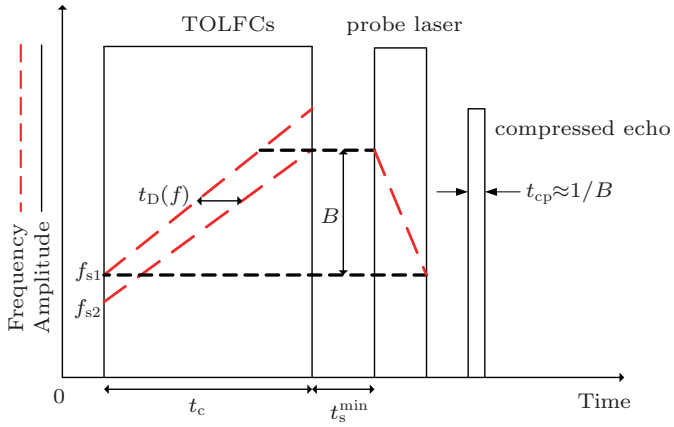


Fig. 5. (color online) Diagram for the generation of compressed echo.

As shown in Fig. 5, the upper laser called the reference laser and the lower counterpart laser called the control laser interact with each other, thus producing a grating bandwidth B within τ_c. Assume that the start frequency of the reference laser is f_{s1} with linear chirp rate α_1 and the start frequency of the control laser is f_{s2} with linear chirp rate α_2, the spectral grating bandwidth B can be expressed as

$$B = \tau_c \alpha_2 - (f_{s1} - f_{s2}), \tag{21}$$

where $B \leq B_{inhom}$, B_{inhom} is the bandwidth of the SHB inhomogeneous broadening absorption spectrum.

The delay time between the first two linear chirp lasers at certain frequency f can be given as

$$\begin{aligned}\tau_D(f) &= (f - f_{s1})\left[(\alpha_1 - \alpha_2)/(\alpha_1\alpha_2)\right] \\ &\quad + \left[(f_{s1} - f_{s2})/\alpha_1\right].\end{aligned} \tag{22}$$

After the spectral grating is produced and delay time τ_s, a probe laser scans the REIC with chirp rate $\alpha_3 = (\alpha_1\alpha_2)/(\alpha_2 - \alpha_1)$. Due to the compression effect of the chirp lasers, a pulse compression echo $\tau_{cp} \approx 1/B$ appears.

The compressed echo can be regarded as the aggregation of numerous single photon echoes which occur from f_{s1} to $f_{s1} + B$,[2,4] but it has no explicit expression in the previous papers. Therefore, we are interested in finding a mathematical expression describing the relationship between the single photon echo and the compressed echo.

According to Fig. 5, the chirp lasers can be treated as numerous discrete frequency rectangle pulses with different amplitudes shot into the crystal as shown in Fig. 6. The electric amplitude of each rectangle pulse must follow the envelope of the chirp signal, namely,

$$\begin{aligned}E_{0j}(n) &= E_{j0}\exp\left\{\mathrm{i}\omega_{sj}\left[n\left(t'_j - t_j\right)\right]\right. \\ &\quad \left. + \mathrm{i}\pi\alpha_j[n\left(t'_j - t_j\right)^2]\right\},\end{aligned} \tag{23}$$

where $j = 1,2,3$, $n = 1,2,\ldots,N$, E_{j0} is the initial amplitude of each chirp laser, and ω_{sj} is the start frequency of the j-th chirp laser.

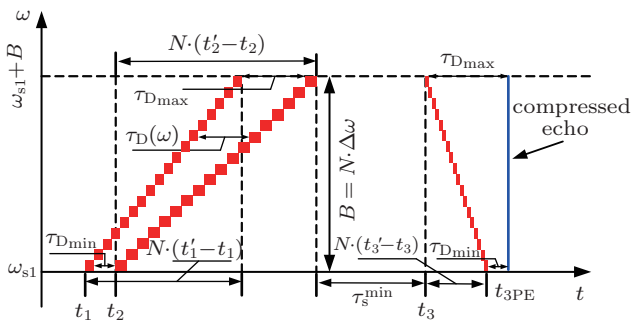


Fig. 6. (color online) Diagram for generation of compressed echo. Each chirp laser is regarded as numerous discrete frequency rectangle pulses, where N is the amount of pulses and $\Delta\omega$ is the frequency step.

Therefore, the model of the compressed echo can be written as

$$\begin{aligned}E_{cp}(t) &= \sum_{n=1}^{N}\left\{-\wp N_{atom} L\left[\omega_{ab} + \omega_{s1} + (n-1)\Delta\omega\right]/2\varepsilon c\right. \\ &\quad \times \left[(R_{01}R_{02}R_{03})/(R_1R_2R_3)\right] w(t_1) \\ &\quad \times \cos\left[\delta\omega(t - t_{3PE})\right] \mathrm{e}^{-\frac{(t-t_{3PE})^2\delta\omega_D^2}{4}} \\ &\quad \times \sin\left(R_1 t'_1\right)\sin\left[R_2\left(t'_2 - t_2\right)\right]\sin\left[R_3\left(t'_3 - t_3\right)\right] \\ &\quad \times \mathrm{e}^{-\left\{\left[t_3 + (N-n)\left(t'_3 - t_3\right)\right] - \left[t'_2 + (n-1)\left(t'_2 - t_2\right)\right]\right\}/T_1} \\ &\quad \times \mathrm{e}^{-\left\{\left[t_2 + (n-1)\left(t'_2 - t_2\right)\right] - \left[t'_1 + (n-1)\left(t'_1 - t_1\right)\right]\right\}/T_2} \\ &\quad \left. \times \mathrm{e}^{-\left[t - \left(t_3 + (N-n+1)\left(t'_3 - t_3\right)\right)\right]/T_2}\right\},\end{aligned} \tag{24}$$

where $R_{0j} = \wp E_{0j}(n)/\hbar$ and $R_j = \sqrt{R_{0j}^2 + \Delta^2}$, $j = 1,2,3$.

3. Simulation results

The simulation is performed to demonstrate the compressed echo which is the aggregation of numerous single photon echoes with different frequencies. All the parameters used are cited from Ref. [3]. The population lifetime T_1 is set as 10 ms and the coherence time $T_2 = 150$ μs. The inhomogeneous width $\delta\omega_D$ is set as 40 GHz and the thickness of the medium $L = 2.5$ mm. The grating bandwidth B is set as 1.2 GHz and the amount of discrete number $N = 1.2 \times 10^9$, namely, the frequency step $\Delta\omega = 1$ Hz. The start frequency ω_{s1} is set as 80 MHz and the frequency shift $\delta\omega$ is set as 50 MHz. The durations of the three chirp lasers are 800 μs, 788.7 μs, and 12 μs, respectively. The chirp rate of each laser should follow $\alpha_3 = (\alpha_1\alpha_2)/(\alpha_2 - \alpha_1)$, namely,

$$\begin{aligned}\frac{N\Delta\omega}{N\left(t'_3 - t_3\right)} &= \left[\frac{(N\Delta\omega)^2}{N^2\left(t'_1 - t_1\right)\left(t'_2 - t_2\right)}\right] \\ &\quad \times \left[\frac{N\Delta\omega}{N\left(t'_2 - t_2\right)} - \frac{N\Delta\omega}{N\left(t'_1 - t_1\right)}\right]^{-1}.\end{aligned} \tag{25}$$

The minimum time delay τ_s^{min} between the engraving process and the probe laser is set as 300 μs. The compressed echo will appear at 1.123 ms, as shown in Fig. 7.

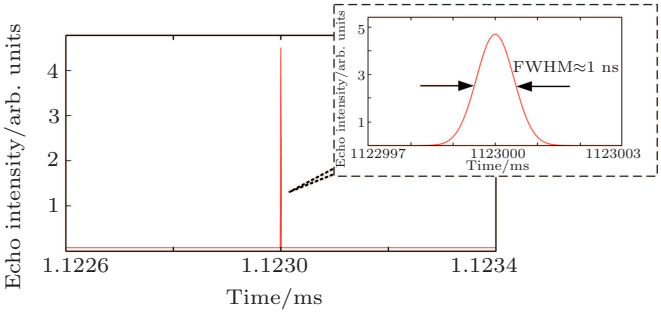


Fig. 7. (color online) Simulation of compressed echo whose full width at half magnitude (FWHM) is 1 ns. The time width τ_{cp} of the compressed echo is obviously narrow, which approaches the theoretical value $1/B \approx 0.83$ ns. Our simulation result is quite close to the experiment result (FWHM is 0.9 ns) in Ref. [3].

Meanwhile, we can calculate the intensity and efficiency of the compressed echo in Ref. [3]. They used yttrium orthosilicate (Er^{3+}:YSO) crystal ($T_2 \sim 150$ μs and $T_1 \sim 11$ ms) to produce the compressed echo. The time delay at the same frequency $\tau_D(f)$ is set as 11.3–12.42 μs, while the minimum time delay τ_s^{min} is set as 0.3 ms, and the maximum time delay τ_s^{max} is set as 1.1 ms. The stimulated compressed echo can maintain $\sim 67.62\%$ intensity and $\sim 28.5\%$ efficiency according to Eqs. (17) and (20).

Now, we propose some approaches for improving the intensity and efficiency of the compressed echo in arbitrary waveform generation based on Eqs. (17), (20), and (24).

The first method is controlling the time delay τ_D. Equation (17) shows that a larger time delay between pulse #1 and pulse #2 will decrease the intensity of the photon echo. The time delay τ_D between the reference laser and the control laser can be rewritten in a discrete form as

$$\tau_D = \left[t_2 + (n-1)\left(t_2' - t_2\right)\right] - \left[t_1' + (n-1)\left(t_1' - t_1\right)\right]. \quad (26)$$

The time delay τ_D has two items in Eq. (22) which are related to the start frequencies and the chirp rate of TOLFCs.

As shown in Figs. 8–10, we find that decreasing the difference of TOLFCs' start frequencies and the difference of the chirp rates, and utilizing higher chirp rate lasers will achieve higher echo's intensity.

Another method is to reduce the time delay τ_s^{min} between the engraving process and the probe step. Equation (17) shows that a larger time delay between pulse #2 and pulse #3 will decrease the compressed echo's intensity as well. The time delay τ_s^{min} between the engraving process and the probe step can be rewritten in a discrete form as

$$\tau_s^{min} = t_3 - \left[t_2' + (N-1)\left(t_2' - t_2\right)\right]. \quad (27)$$

As mentioned in Refs. [2], [3], and [6]–[8], the chirp rate of the probe laser is much higher than that of the engraving lasers (Eq. (2) of Ref. [2]) and the transform time τ_s^{min} depends on the reaction speed of the arbitrary waveform generator and the optical phase lock loop.

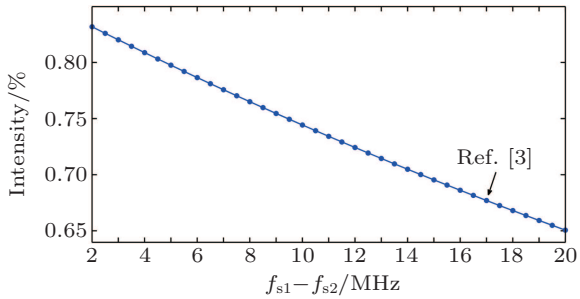


Fig. 8. (color online) Relationship between difference of start frequency $(f_{s1}-f_{s2})$ and compressed echo's intensity.

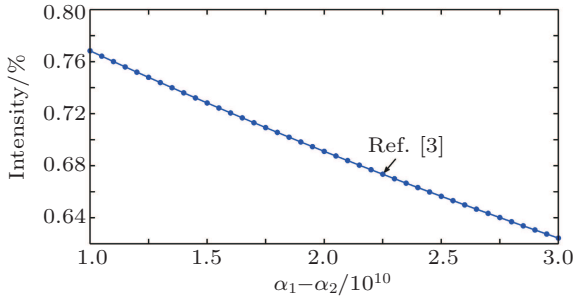


Fig. 9. (color online) Relationship between difference of chirp rate $(\alpha_1 - \alpha_2)$ and compressed echo's intensity.

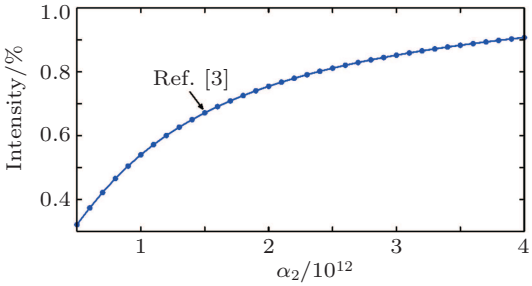


Fig. 10. (color online) Relationship between chirp rate α_2 and compressed echo's intensity.

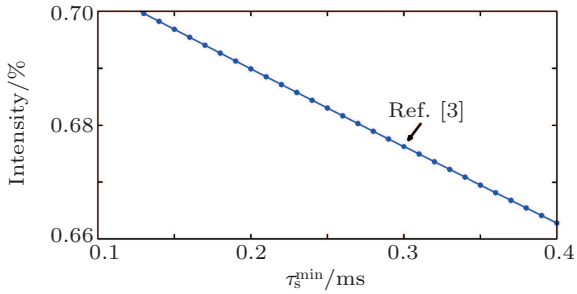


Fig. 11. (color online) Relationship between τ_s^{min} and compressed echo's intensity.

As shown in Fig. 11, the larger time delay τ_s^{min} will decrease the compressed echo's intensity. Therefore, we should increase the reaction speed of the experimental instruments to shorten the time delay for keeping a high intensity of the compressed echo.

Increasing the optical thickness is also a useful method. According to Eq. (20), the efficiency of 3PE is related to the optical thickness. The efficiency increases with the increase of the optical thickness. The optical thickness αL is the product of absorption coefficient α and thickness L of the REIC.

It is unpractical to replace a much thicker REIC in the cryogenic equipment frequently. Thus, it is reasonable to increase the absorption coefficient α and it can be expressed as[12]

$$\alpha(f) = \alpha_0 \pi G(f) / \left[T_2 \sqrt{1 + |R_0|^2 T_1 T_2}\right]. \quad (28)$$

Here α_0 is the resonant absorption coefficient, and $G(f)$ is the laser frequency f which follows a Gaussian distribution. Obviously, it is efficient to scan lasers around the center frequency

f_0 of the inhomogeneously broadened spectrum to increase the absorption coefficient α as shown in Fig. 12.

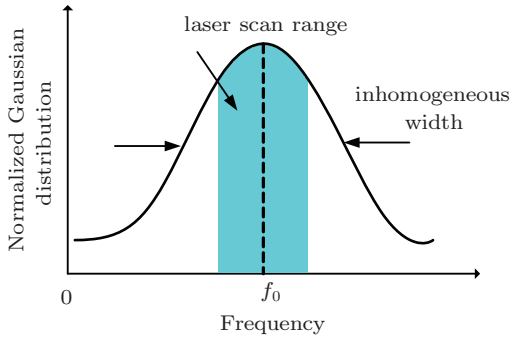


Fig. 12. (color online) Diagram for laser scan range in inhomogeneously broadened spectrum.

The proper choice of REIC is also necessary. Different rare-earth-ion-doped crystals possess different T_2 and T_1. The coherence time T_2 is determined by $T_2 = 1/(\pi\Gamma_h)$, where Γ_h is the homogeneous width of the medium. With the decrease of the temperature (ultralow temperature of 3–4 K), the line shape of the homogeneous broadening becomes sharper, which makes Γ_h narrower and enhances T_2 at the same time.[16,17] The population lifetime T_1 is decided by the wavelength of the excited state in the two-level system. According to Eq. (17), larger coherence time T_2 and population lifetime T_1 make the photon echo have a tiny attenuation of intensity but it does not mean that the larger the better. According to Eq. (28), larger T_1 and T_2 will decrease the absorption coefficient α, which may reduce the efficiency of 3PE.

Take the case in Ref. [3] for example; if we replace Er^{3+}:YSO with Tm^{3+}:YAG ($T_2 \sim 20$ μs and $T_1 \sim 10$ ms) and do not change other parameters, we will find that the intensity and efficiency of the compressed echo are 7.9% and 8%, respectively, which are far smaller than those with the Er^{3+}:YSO crystal.

Larger coherence time T_2 and excitation lifetime T_1 may reduce the efficiency of 3PE, but they can lead to a higher intensity that offsets the increase of $e^{-\alpha L}$. Therefore, the crystal with larger coherence time T_2 and excitation lifetime T_1 is beneficial to produce the compressed echo, which will be more suitable for the arbitrary waveform generation and optical storage based on the 3PE technology.[3,5]

4. Conclusion and perspectives

We have proposed a novel model of compressed echo. We first deduced the expression of 3PE based on the Bloch equations and verified that larger time delay of the input pulses will decrease the echo's intensity. Furthermore, the efficiency of 3PE is a sine-like function with the increase of the rephasing pulse's area and that of the optical thickness. Then, we gave the relationship between the single photon echo and the compressed echo. The novel model of compressed echo predicts the possibility of achieving high intensity and efficiency of the compressed echo. According to this model, we gave several suggestions for improving the compressed echo. These results and recent results of echoes in inverted media serve as a motive to further study the possibility of obtaining a highly efficient and strong echo.

References

[1] Chang T, Tian M and Babbitt W 2004 *J. Lumin.* **107** 138
[2] Renner C J, Reibel R R, Tian M, Chang T and Babbitt W 2007 *J. Opt. Soc. Am. B* **24** 2979
[3] Damon V, Crozatier V, Chaneliere T, Gouet J Le and Lorgere I 2010 *J. Opt. Soc. Am. B* **27** 524
[4] Crozatier V, Tian M, Barber Z W and Babbitt W 2004 *IEEE J. Quantum. Electron.* **40** 1450
[5] Mitsunaga M 1992 *Opt. Quantum. Electron.* **24** 1137
[6] Barber Z W, Tian M, Reibel R R and Babbitt W 2002 *Opt. Express* **10** 1145
[7] Ma X, Wang S, Zhang S, Zhang S and Liang Y 2015 *IEEE Commun. Lett.* **19** 179
[8] Ma X, Wang S, Liang Y and Shan Y 2015 *Appl. Opt.* **54** 2891
[9] Sangouard N, Simon C and Minar J 2010 *Phys. Rev. A* **81** 2333
[10] Mossberg T W, Kachru R, Hartmann S R and Flusberg A M 1979 *Phys. Rev. A* **20** 1976
[11] Azadeh M, Cornish S C, Babbitt W and Tsang L 1998 *Phys. Rev. A* **57** 4662
[12] Meystre P and Sargent M III, 2007 *Elements of Quantum Optics* (4^{th}Edn.) (New York: Springer Press) pp. 281–288
[13] Chang T, Tian M and Babbitt W 2004 *J. Lumin.* **107** 129
[14] Gradshteyn I S and Ryzhik I M 2007 *Table of Integrals, Series, and Products* (7^{th} Edn.) (New York: Elsevier Academic Press)
[15] Mitsunaga M and Brewer R G 1985 *Phys. Rev. A* **32** 1605
[16] Chen L, Ma X R and Wang W 2013 *Chin. Phys. B* **22** 064213
[17] Ma X R, Zhang S Y and Zhang S G 2014 *Chin. Phys. B* **23** 060304